Original Article

http://dx.doi.org/10.3348/kjr.2012.13.4.458
pISSN 1229-6929 · eISSN 2005-8330
Korean J Radiol 2012;13(4):458-466

Korean Journal of Radiology
KJR

Differential Diagnosis of Axillary Inflammatory and Metastatic Lymph Nodes in Rabbit Models by Using Diffusion-Weighted Imaging: Compared with Conventional Magnetic Resonance Imaging

Junping Wang, PhD[1], Qian Liao, MD[2], Yunting Zhang, PhD[1], Chunshui Yu, PhD[1], Renju Bai, PhD[1], Haoran Sun, PhD[1]

[1]Department of Radiology, Tianjin Medical University General Hospital, Tianjin 300052, China; [2]Department of Radiology, The First Affiliated Hospital of Nanchang University, Jiangxi 330006, China

Objective: This experiment aims to determine the diagnostic value of diffusion-weighted imaging (DWI) in the differentiation of axillary inflammatory lymph nodes from metastatic lymph nodes in rabbit models in comparison with conventional magnetic resonance imaging (MRI).

Materials and Methods: Conventional MRI and DWI were performed at 4 weeks after successful inoculation into the forty female New Zealand white rabbits' mammary glands. The size-based and signal-intensity-based criteria and the relative apparent diffusion coefficient (rADC) value were compared between the axillary inflammatory lymph nodes and metastatic lymph nodes, with histopathological findings as the reference standard. Receiver operating characteristic (ROC) curve analysis was performed to evaluate the diagnostic performance of the aforementioned criteria and rADC value in differentiating the axillary inflammatory lymph nodes from metastatic lymph nodes.

Results: Thirty-two axillary inflammatory lymph nodes and 46 metastatic ones were successfully isolated and taken into pathological analysis. The differences of the aforementioned criteria between the two groups were not statistically significant ($p > 0.05$). However, the rADC value of the inflammatory lymph nodes (0.9 ± 0.14) was higher than that of metastatic ones (0.7 ± 0.18), with significant difference ($p = 0.016$). When the rADC value was chosen as 0.80, the area under the ROC curve is greater than all other criteria, and the sensitivity, specificity, accuracy, positive predictive value, and negative predictive value for differentiating two groups were 86.2%, 79.3%, 81.2%, 84.2%, and 85.6%, respectively.

Conclusion: Diffusion-weighted imaging is a promising new technique for differentiating axillary inflammatory lymph nodes from metastatic lymph nodes. Compared with routine magnetic resonance sequences, DWI could provide more useful physiological and functional information for diagnosis.

Index terms: *Axillary lymph node; Diffusion-weighted imaging; Relative ADC; Animal model*

Received October 17, 2011; accepted after revision January 10, 2012.
Supported by a grant from Science and Technology Fund of Tianjin Public Health Bureau, China (No. 09KZ105).

Corresponding author: Junping Wang, PhD, Department of Radiology, Tianjin Medical University General Hospital, Anshan Road 154, Heping District, Tianjin 300052, China.
• Tel: (8622) 60363760 • Fax: (8622) 60362990
• E-mail: wangjunping_tj@163.com

INTRODUCTION

Axillary lymph node involvement is the most common route of breast cancer metastases, and is an essential prognostic factor and an important determinant in the treatment of patients with breast cancer (1-4). Axillary lymph nodes dissection with histopathological examination of the surgical specimen is regarded as the gold standard for detecting involvement of the lymph nodes (1, 2). Complications, such as seroma formation, numbness, limitation of shoulder movement, and lymphedema, have

Korean Journal of Radiology
KJR

been reported (5-7). Thus, a noninvasive technique that assists in the accurate identification of axillary lymph node metastases before operation would be beneficial by helping surgeons to choose appropriate treatment regimens to improve the clinical outcome and minimize complications associated with unnecessary lymphadenectomy.

With magnetic resonance imaging (MRI), computed tomography, and ultrasonography techniques, the preoperative assessment of axillary lymph node status is based mainly on measurement of nodal dimensions, such as maximum long-axis diameter, short-axis diameter or long/short-axis ratio, but these techniques are somewhat limited. In addition, morphologic criteria (e.g., shape, thickened lobular cortex, displacement and/or absence of fatty hilus), enhancement patterns, and grouping of lymph nodes are further important parameters (8-11). All these criteria remain controversial, and recommendations for differentiation between metastatic and non-metastatic lymph nodes vary widely.

Diffusion-weighted imaging (DWI) facilitates the noninvasive characterization of various tissues on the basis of their water diffusion properties. Any architectural changes in the proportion of extracellular to intracellular water protons will alter the diffusion coefficient of the tissue (12-15), thus providing information about the biophysical properties of tissues *in vivo*. Quantitative measurement of apparent diffusion coefficient (ADC) could reflect the degree of restriction of diffusion of different tissues. Although accumulating evidence indicated that the ADC value may improve the accuracy for diagnosing metastatic lymph nodes in uterine cervical cancer and head and neck cancer (16-20). However, whether ADC value is potentially useful in detecting axillary metastatic lymph nodes is less clear. There has only been one report evaluating axillary lymph nodes by diffusion-weighted MRI in patient with breast cancer: the results of which concluded that the differences in the ADC value between metastatic and non-metastatic nodes were not significant (21). In clinical studies, DWI may find numerous lymph nodes, although for the most part it is extremely difficult to produce accurate pathology results from images for each lymph node, one by one. We performed our present study in order to have the exact pathological result for a lymph node, and the purpose of this experiment was to investigate the feasibility of DWI technique to discriminate between axillary inflammatory and metastatic lymph nodes in rabbit models.

MATERIALS AND METHODS

Animal Model Preparation

This experiment was approved by the animal care committee at Tianjin Medical University General Hospital. Forty healthy female New Zealand white rabbits offered by the Laboratory Animal Center of Tianjin Medical University (weighing 2.0-2.5 kg) were randomly divided into two equal groups. The rabbits were allowed food and water ad libitum. After the rabbits were anesthetized, by injecting 3% soluble pentobarbitone into the abdominal cavity at a dose of 1 mL/kg, 0.5 mL Complete Freund's adjuvant (brought from Sigma Corporation, St. Louis, MO, USA) was injected into the rabbits' mammary glands underneath the lateral upper quadrant of the bilateral second nipple so as to set up the axillary inflammatory reactive hyperplastic lymph node models, and 1 mL VX2 tumor tissue suspension (provided by Pathology faculty of China Xiehe Medical University) was inoculated into another group of rabbits into the same location as that of the axillary metastatic lymph node models described previously (22). The rabbits were sacrificed immediately after MRI examination and imaging and histopathological comparisons were conducted.

MRI Scanning Protocol and Parameters

All MRI examinations were performed with a 1.5 T superconducting magnet (Twinspeed Infinity with Excite II, GE Medical Systems, Milwaukee, WI, USA) and a knee coil to improve the resolution. MRI covered bilateral axillary fossa areas were acquired 4 weeks after inoculation for the axillary inflammatory and metastatic lymph nodes. The anesthetic regimen used for implantations were also used for MRI examination. All of the animals were imaged in the prone position with elevated arms. Prior to DWI, axial and sagittal T2WI, fast spin-echo sequences with or without fat suppression (TR/TE, 3500/68 msec; slice thickness, 3 mm; interslice gap, 0.5 mm; field of view, 15 x 15 cm; matrix, 256 x 224; number of excitation, 4; echo train length, 15); and axial and sagittal T1WI spin-echo sequences with or without fat suppression (TR/TE, 520/11 msec; matrix, 256 x 160, the remaining parameters were the same as those of T2WI) were obtained. Transverse DWI were obtained using array spatial sensitivity encoding technique (ASSET) and free-breathing short TI inversion recovery single-short echo-planar-imaging (STIR-SS-EPI) sequence with the following parameters (TR/TE, 5000/67.3 msec; slice thickness, 3 mm; interslice gap, 0.5 mm; field of view, 15 x 15 cm; matrix,

128 x 128; number of excitation, 4, parallel factor, 2) with b values of 0 and 800 s/mm^2. The DWI gradients were applied in all three orthogonal directions, which coincided with the slice-selective, phase-encoding, and readout directions. The scanning time of all sequences was less than 25 minutes.

Measurements on MRI and Image Analysis

All MRI were assessed with an emphasis placed on the bilateral axillary fossa lymph nodes. Two experienced radiologists, who were blinded to the histological findings, evaluated all the MRI by consensus.

Both the axillary inflammatory or metastatic lymph nodes with the short-axis diameter equal or greater than 5 mm were included in our study. The long-axis (L) and short-axis diameter (S) were measured on the corresponding maximum section of each lymph node on axial T2WI, respectively, and the long/short-axis ratio (L/S) was calculated. The signal intensity on T2WI and DWI (S_{T2WI}, S_{DWI}) of each selected lymph node was measured. The ADC maps were calculated on a pixel-by-pixel basis by using built-in software (AW4.2 Functool; GE Healthcare, Milwaukee, WI, USA). We used the corresponding central slice of each lymph node on the ADC map, a round or elliptical region of interest (ROI) covering about 3/4 of the entire area of the selected lymph node attempting to avoid inclusion of the margins; while T2W imaging was used as the anatomical reference. The relative ADC (rADC) value was calculated by $ADC_{lymph\ node}$/$ADC_{reference\ site}$, and the dorsal muscle was determined to be the reference site for the rADC. The ROI with the same size was also drawn on the center area of the ipsilateral dorsal muscle at the same level of each lymph node on the ADC map. The area of the ROI in the selected axillary lymph nodes was 25-150 mm^2, according to their different sizes. All the values were averaged from three-time measurements and expressed as the mean ± standard deviation.

Statistical Analysis

Statistical analyses were performed by using Statistical Product and Service Solutions (SPSS, version 18.0, Chicago, IL, USA). All the measurements were in normal distribution. Differences of L, S, L/S, signal intensity on T2WI (SI_{T2WI}), signal intensity on DWI (SI_{DWI}), and the rADC value between the axillary pathologically proven inflammatory lymph nodes and the malignant lymph nodes were compared respectively, using independent *t* test with a level of *p* value less than 0.05 considered statistically significant. A receiver operating characteristic (ROC) curve analysis was used to compare the diagnostic performance of rADC value and each of the size-based criteria and signal-intensity-based criteria for the differentiation of the axillary inflammatory and metastatic lymph nodes. Thereafter, the appropriate areas under the curve were evaluated and compared. From the ROC curve analysis, The Youden's index was used in determining the optimal threshold rADC value for differentiating axillary inflammatory from metastatic lymph nodes. Once the optimal criterion was obtained, we would calculate the sensitivity, specificity, accuracy, and positive and negative predictive values (PPV, NPV) using the corresponding resulting threshold.

RESULTS

Pathological Results

According to the MRI, a total of 78 lymph nodes in bilateral axillary fossa with a short-axis diameter equal to or larger than 5 mm, including 32 inflammatory and 46 metastatic ones, were successfully isolated and taken into analysis. The inflammatory lymph nodes had smooth pinkish-grey surfaces, while the metastatic lymph nodes had shaggy pale-grey surfaces with a fish like texture (Fig. 1). Light microscopy showed inflammatory lymph nodes with abundant lymphocytes and plasmacytes infiltration, reactive hyperplasia, and fibrous connective tissue proliferation (Fig. 1). Histopathologic analysis of the metastatic lymph nodes revealed that nest-like gathered tumor cells with enlarged irregular nuclei or pathological mitotic figures, plasma cells, and (rarely) lymphocytes were observed in the nodes (Fig. 1).

Image Characteristics of the Two Group Lymph Nodes

When ASSET and STIR were used, image distortion was significantly reduced to a minimum, and DWI was of diagnostic quality in all cases; no cases were excluded from our study.

All of the axillary inflammatory and metastatic lymph nodes were isointense on T1WI, hyperintense relative to that of adjacent skeletal muscle on T2WI and DWI, and all of the signal intensity of the selected lymph nodes was homogeneous without visible necrosis and cystic degeneration. On pseudo-color ADC maps, the inflammatory lymph nodes showed as green or yellow regions (Fig. 2), while the metastatic ones manifested as blue regions (Fig. 3).

Korean Journal of Radiology
KJR

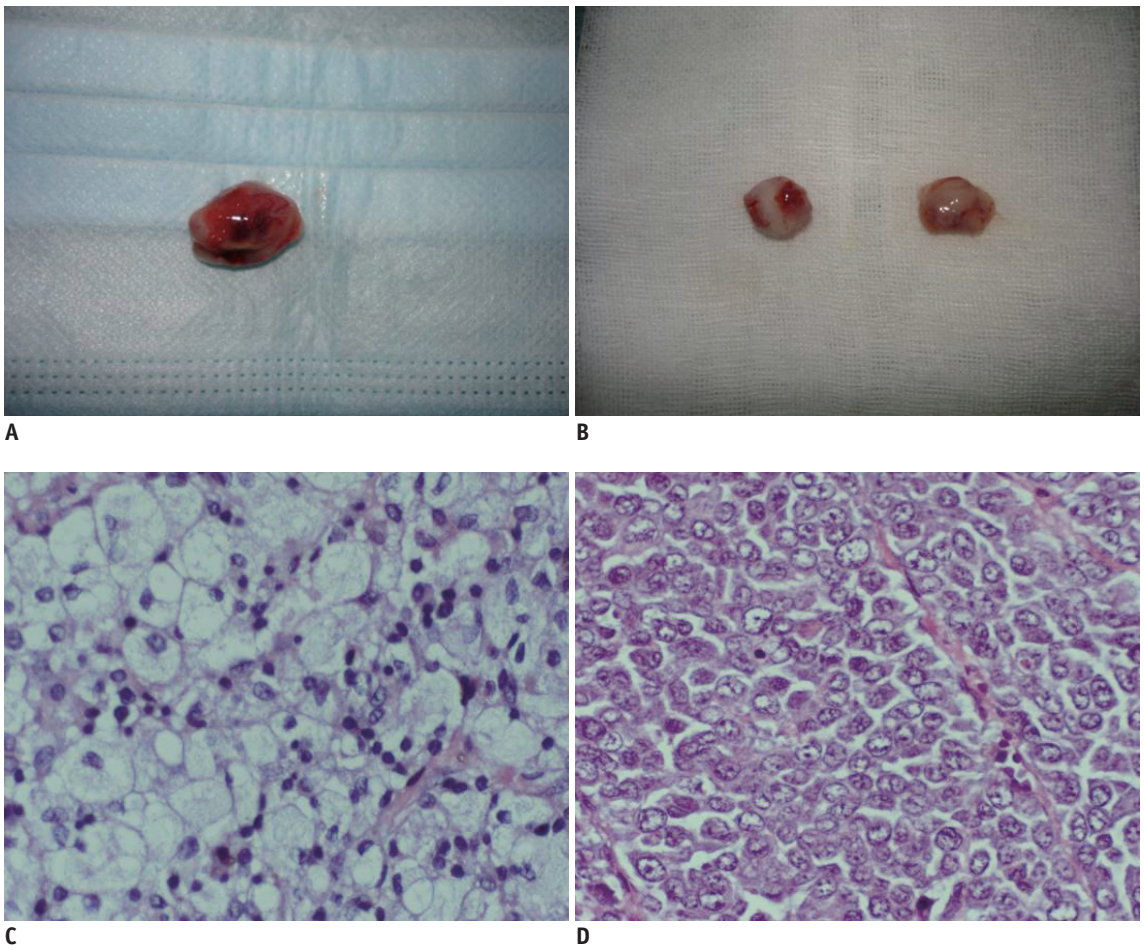

Fig. 1. Manifestations of gross specimen and histopathological examination of axillary inflammatory and metastatic lymph nodes. Gross specimen of axillary inflammatory lymph node show that they have smoothly pinkish-grey surfaces and abundant vessels **(A)**, while axillary metastatic lymph nodes appear to have shaggy pale-grey surface with fish like texture **(B)**. Histopathological examination (H & E, x 200) shows inflammatory cell infiltration and cells arrangement sparsely with intercellular substance edema **(C)**, while tumor cells deposit within metastatic lymph node, and enlarged nuclei, hyperchromatism, high nuclear-to-cytoplasmic ratio, and pathological mitotic figure are observed **(D)**.

Comparison of Size-Based Criteria, Signal-Intensity-Based Criteria, and rADC Value between the Two Group Lymph Nodes

The mean value of L, S, L/S, SI_{T2WI}, SI_{DWI}, and rADC of the axillary inflammatory and metastatic lymph nodes were 10.21 ± 0.24 mm, 5.00 ± 0.25 mm, 1.98 ± 0.13 mm, 380.25 ± 28.45 mm, 878.64 ± 51.38 mm, and 0.9 ± 0.14 mm and 13.72 ± 0.19 mm, 8.77 ± 0.32 mm, 1.49 ± 0.15 mm, 452.11 ± 60.78 mm, 975.44 ± 33.62 mm, and 0.7 ± 0.18 mm, respectively. Each of the size-based criteria and signal-intensity-based criteria between two groups showed no statistically significant difference; however, the rADC value of the inflammatory lymph nodes was higher than that of metastatic ones in axillary fossa (0.9 ± 0.14 mm vs. 0.7 ± 0.18 mm) with b values of 0 and 800 s/mm^2: the difference between the two groups was statistically significant (Table 1).

The appropriate area under the ROC curve for L, S, L/S, SI_{T2WI}, SI_{DWI}, and rADC value was 0.67, 0.70, 0.57, 0.49, 0.38, and 0.82, respectively (Fig. 4). Since the area for the rADC value was greater than those of all other criteria, the former was used as the representative index for differentiation of inflammatory from metastatic lymph nodes. When choosing 0.80 as diagnostic optimal threshold of the rADC value, the Youden index was the maximum, and its sensitivity, specificity, accuracy, PPV, and NPV was 86.2%, 79.3%, 81.2%, 84.2%, and 85.6%, respectively.

DISCUSSION

A noninvasive technique that accurately assesses lymph node metastasis would be of great benefit to patients with breast cancer, since surgical lymph node dissection, which is regarded as the gold standard method for the diagnosis of lymph node metastasis, will increase the cost and time

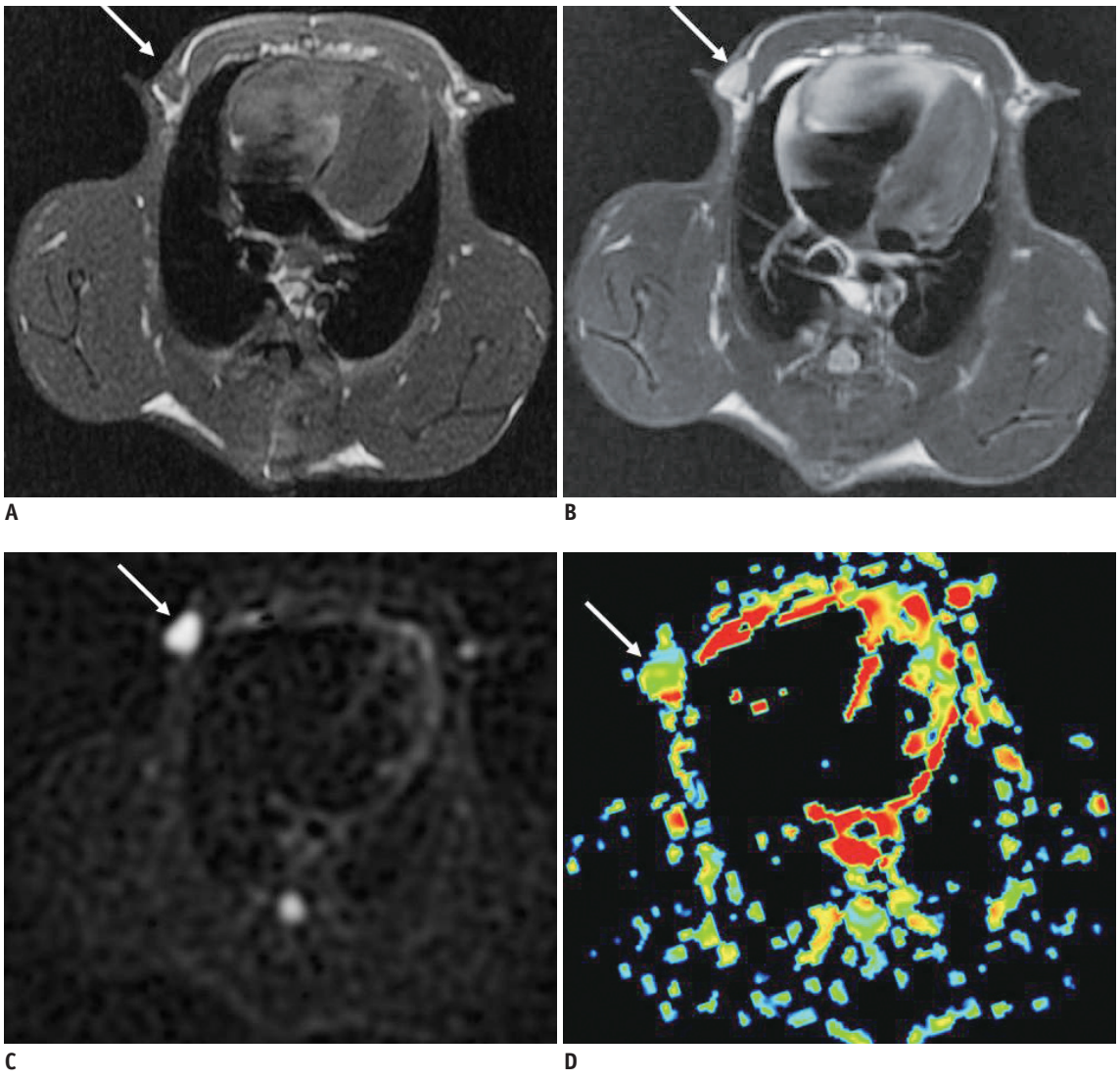

Fig. 2. Appearance of conventional MRI, diffusion-weighted imaging and apparent diffusion coefficient map of axillary inflammatory lymph node.
Inflammatory lymph node in right axillary fossa on axial T2WI shows iso-intensity with unclear borderline (arrow) **(A)**. Axial T2WI shows high signal intensity (arrow) **(B)**. Corresponding diffusion-weight imaging demonstrates homogeneous high signal intensity (arrow), and conspicuity in identification of same node is higher in this image compared with T2WI **(C)**. Node is depicted as area of green in most part, with scattered yellow dots (arrow) on pseudo-color apparent diffusion coefficient map, and relative apparent diffusion coefficient value of this node is 0.86 **(D)**.

of diagnosis and the risk of complications to the patient (4, 6). Therefore, if we were able to determine preoperatively whether metastases to the axillary lymph nodes were present or not, we would be able to avoid unnecessary lymphadenectomy and, meanwhile, improve treatment management and minimize the surgical complications and costs. Traditional size criteria indicated that nodes with short-axis diameter of longer than 10 mm were defined as metastasis (23, 24). However, investigators have proven that this criteria is inaccurate (3, 4), and based on the size criteria, the sensitivity in the diagnosis of metastatic nodes is low (53-62%) (25). Moreover, Obwegeser et al. (26) reported that, in histological analysis of 1249 axillary lymph nodes in 71 patients with breast cancer, 13.7% of metastatic nodes were 5-9 mm in short-axis diameter. In our study, there was no statistical difference between L, S, and L/S between the axillary inflammatory and metastatic lymph nodes, respectively, and neither was the signal intensity on T2WI, in agreement with the results obtained by Som (27).

DWI, which is noninvasive, does not require contrast medium administration, and it does not involve ionizing radiation, an important MRI technique that enables the radiologist to move from morphological to functional

Korean Journal of Radiology
KJR

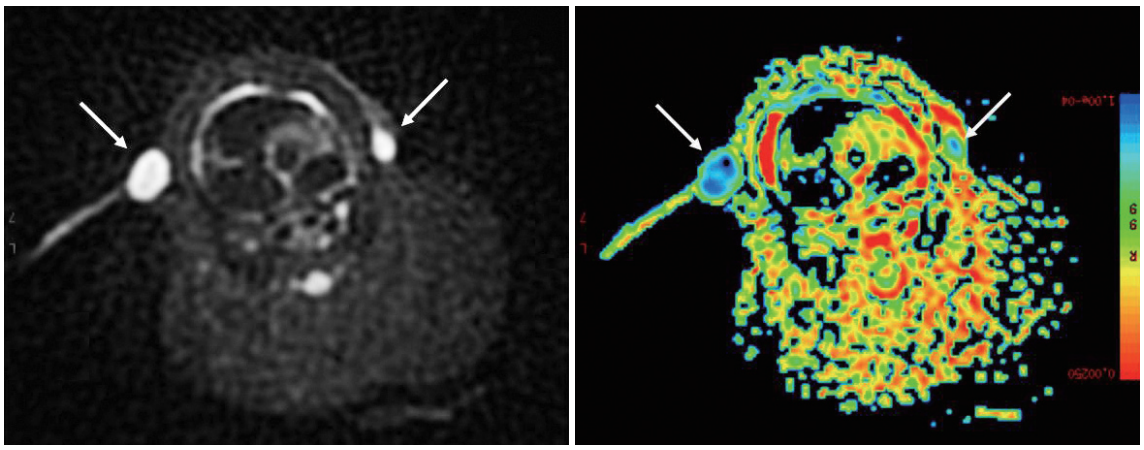

A B

Fig. 3. Manifestation of diffusion-weighted imaging and apparent diffusion coefficient map of axillary metastatic lymph nodes. Two axillary metastatic lymph nodes in bilateral axillary fossa on axial diffusion-weighted imaging show obviously homogeneous high signal intensity with clear margin (arrow) **(A)**. Both of them demonstrated as areas of blue on corresponding apparent diffusion coefficient map (arrow), and relative apparent diffusion coefficient value of left and right nodes is 0.60, 0.55, respectively **(B)**.

Table 1. Comparison of L, S, L/S, SI_{T2WI}, and SI_{DWI} between Group Lymph Nodes

Measurements	Inflammatory Lymph Nodes (n = 32)	Metastatic Lymph Nodes (n = 46)	t	*P*
L (mm)	10.2 ± 0.24	13.7 ± 0.19	-1.305	0.128
S (mm)	5.0 ± 0.25	8.8 ± 0.32	-1.962	0.079
L/S	2.0 ± 0.13	1.5 ± 0.15	1.107	0.209
SI_{T2WI}	380.3 ± 28.45	452.1 ± 60.78	-0.967	0.312
SI_{DWI}	878.6 ± 51.38	975.4 ± 33.62	-0.741	0.464
rADC value	0.9 ± 0.14	0.7 ± 0.18	4.879	0.016

Note.— L = long-axis diameter, L/S = long/short-axis ratio, S = short-axis diameter, SI_{DWI} = signal intensity on diffusion-weighted imaging, SI_{T2WI} = signal intensity on T2WI, rADC = relative apparent diffusion coefficient

assessment of diseases. The conspicuity in the identification of nodes on DWI was significantly higher than that on T2WI, since the axillary lymph nodes were shown with marked high signal intensities in comparison with the adjacent muscle and surrounding normal vessels on DWI that made it easy to identify (28). However, visual assessment of DWI to differentiate the axillary inflammatory from metastatic lymph nodes was a rather difficult task, as shown in Figure 2 and 3, because both group lymph nodes showed high signal intensities on DWI. In contrast, the ADC values calculated from DWI can provide quantitative analysis of microscopic water diffusivity in the target tissues and can completely exclude the T2 shine-through effect (29). In biological tissue, the ADC values are considered to be mainly influenced by the motion of water molecules in the extracellular space and capillary perfusion. Generally, the larger the b-value is, the greater the degree of signal attenuation from the motion of water molecules is (29, 30). In our study, DWI was performed with a high b-value of 800 s/mm^2, which could evaluate water diffusion more precisely and nearly rule out the effects of capillary perfusion.

The lower ADC value always observed in metastatic lymph nodes could be explained by the histopathological manifestation of the resected specimen. In our study, the VX2 tumor is an anaplastic squamous cell carcinoma and axillary metastatic lymph nodes are replaced by cancer cells, resulting in high cell density and enlarged cell size, which would reduce extracellular spaces; meanwhile, the cancer cells had more organelle, enlarged nuclei, hyperchromatism, and high nuclear-to-cytoplasmic ratio, limiting the diffusion of water molecules in intracellular spaces. These histophatological characteristics resulted in a decrease in the ADC value.

Although many studies have proven the feasibility of ADC for cancer detection in various organs by showing a lower ADC in cancer tissue than in non-cancerous tissue, the mean ADC in each cancer seems to vary greatly according to the studies. For example, the mean ADC of breast cancer ranged from 0.75 x 10^3 mm^2/sec to 1.50 x 10^3 mm^2/sec in previous studies (31-34).

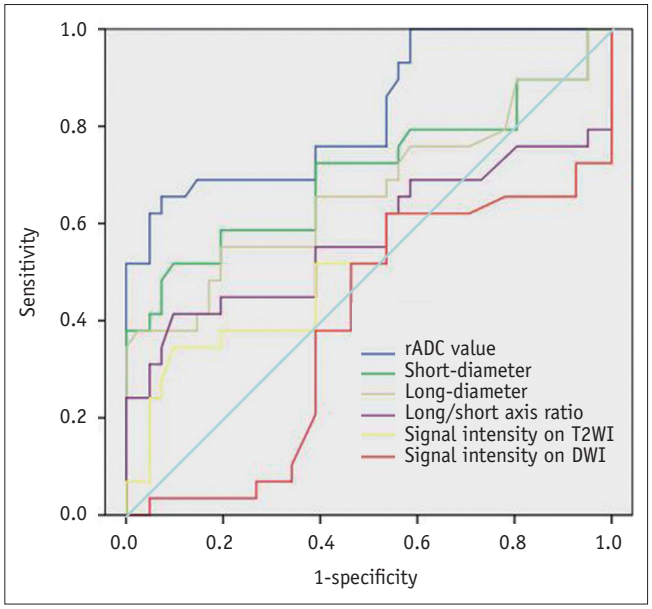

Fig. 4. Graph shows that receiver operating characteristic curve for rADC value is superior to size-based criteria (short-diameter, long-axis diameter, and long/short-axis ratio) and signal intensity on T2WI and DWI for differentiation of inflammatory from metastatic lymph nodes. DWI = diffusion-weighted imaging, rADC = relative apparent diffusion coefficient

There may be two explanations for this variance. First, ADC is variable according to various factors, such as magnetic resonance (MR) acquisition parameters, magnetic field, location and area of ROI, patient age, and body temperature (35, 36). Park et al. (17) suggested that normalization of ADC may reduce this instability of ADC, known as rADC, which is calculated by the formula $ADC_{lesion}/ADC_{reference\ site}$, and their results show that the renal cortex is an appropriate reference site for rADC, and that rADC may improve the accuracy for diagnosing metastatic lymph nodes in uterine cervical cancer. Lin et al. (19) also showed significant differences of rADC between metastatic and non-metastatic lymph nodes that showed no difference in ADC. In our experiment, the coverage of MR examination did not reach the rabbits' kidneys. We presumed that muscle tissue was most extensively distributed in animals' bodies, and the muscle was more generally used as the reference site of rADC value. We used the ipsilateral dorsal muscle of the rabbits in our study at the same level of each lymph node as the reference site of rADC, playing the role of normalization. Generally, the dorsal muscle tissue of rabbits is not vulnerable to injured, and the ADC value is relatively steady. Moreover, axillary lymph nodes and the ipsilateral dorsal muscle are almost located in the same phase-encoding direction. The possible phase-encoding artifacts can be avoided by dividing between them. Our results showed that the rADC value of the axillary inflammatory lymph nodes (0.9 ± 0.14) was higher than that of metastatic ones (0.7 ± 0.18) with significant difference (t = 4.879; p = 0.016), but there was a little overlap between the two groups. When the rADC value chosen as the best performing cutoff was 0.80 (AUC = 0.822), the sensitivity, specificity, accuracy, PPV and NPV of rADC value in differentiating lymph nodes of the two group was 86.2%, 79.3%, 81.2%, 84.2%, and 85.6%, respectively, all greater than that of all size-based criteria of other reports (24, 25). Maybe there were two plausible explanations for this overlap. We found that not all metastatic lymph nodes were entirely replaced by cancer cells; some of them were partially replaced by cancer cells, resulting in metastatic areas with lower ADC and non-metastatic areas with higher ADC, and the ADC value within a lymph node is rather heterogeneous, containing areas of both metastatic and non-metastatic portions. In contrast, in inflammatory lymph nodes, inflammatory cell infiltration, reactive hyperplasia, and fibrous connective tissue proliferation could be seen, which also would limit the diffusion of water molecules, resulting in a decrease in ADC value. ADC has an inherent limitation for differentiating inflammatory lymph nodes from metastatic lymph nodes because ADC is not specific for cancer cells but only reflects tissue diffusivity. Although tissue diffusivity may differ between inflammatory and metastatic lymph nodes, there must be an overlap, as various conditions, such as ischemia and inflammation, also reduce ADC. This overlap cannot be solved by rADC.

This study has several limitations. First, only axillary lymph nodes that had short-axis diameters equal or greater than 5 mm on T2WI were analyzed, the ability of DWI in detecting lymph nodes smaller than 5 mm in short-axis diameter was uncertain, and the ADC measurements on those small nodes would be hampered because of relatively low spatial resolution and signal-to-noise ratio. Second, we did not use a combined evaluation of the rADC value and size-based criteria, which may improve the accuracy of detection of lymph node metastasis further. Third, the animal model in this study is made with VX2 carcinoma, which is a squamous epithelium testicular cancer. Primary breast cancers usually are a kind of adenocarcinoma, and the behavior of metastasis could be different from that of squamous cell cancer, which could lower the clinical implications of this study.

In conclusion, quantitative measurement of rADC values

Korean Journal of Radiology
KJR

had higher accuracy for differentiating axillary inflammatory from metastatic lymph nodes. DWI should be applied in the clinical area owing to its relatively short acquisition time and lack need for the administration of exogenous contrast medium.

REFERENCES

1. Orel SG, Schnall MD. MR imaging of the breast for the detection, diagnosis, and staging of breast cancer. *Radiology* 2001;220:13-30
2. Morrow M. Role of axillary dissection in breast cancer management. *Ann Surg Oncol* 1996;3:233-234
3. Stets C, Brandt S, Wallis F, Buchmann J, Gilbert FJ, Heywang-Köbrunner SH. Axillary lymph node metastases: a statistical analysis of various parameters in MRI with USPIO. *J Magn Reson Imaging* 2002;16:60-68
4. Michel SC, Keller TM, Fröhlich JM, Fink D, Caduff R, Seifert B, et al. Preoperative breast cancer staging: MR imaging of the axilla with ultrasmall superparamagnetic iron oxide enhancement. *Radiology* 2002;225:527-536
5. Pressman PI. Surgical treatment and lymphedema. *Cancer* 1998;83:2782-2787
6. Yeoh EK, Denham JW, Davies SA, Spittle MF. Primary breast cancer. Complications of axillary management. *Acta Radiol Oncol* 1986;25:105-108
7. Shin JH, Choi HY, Moon BI, Sung SH. In vitro sonographic evaluation of sentinel lymph nodes for detecting metastasis in breast cancer: comparison with histopathologic results. *J Ultrasound Med* 2004;23:923-928
8. Shetty MK, Carpenter WS. Sonographic evaluation of isolated abnormal axillary lymph nodes identified on mammograms. *J Ultrasound Med* 2004;23:63-71
9. Krishnamurthy S, Sneige N, Bedi DG, Edieken BS, Fornage BD, Kuerer HM, et al. Role of ultrasound-guided fine-needle aspiration of indeterminate and suspicious axillary lymph nodes in the initial staging of breast carcinoma. *Cancer* 2002;95:982-988
10. Steinkamp HJ, Cornehl M, Hosten N, Pegios W, Vogl T, Felix R. Cervical lymphadenopathy: ratio of long- to short-axis diameter as a predictor of malignancy. *Br J Radiol* 1995;68:266-270
11. Roth Y, Tichler T, Kostenich G, Ruiz-Cabello J, Maier SE, Cohen JS, et al. High-b-value diffusion-weighted MR imaging for pretreatment prediction and early monitoring of tumor response to therapy in mice. *Radiology* 2004;232:685-692
12. Squillaci E, Manenti G, Cova M, Di Roma M, Miano R, Palmieri G, et al. Correlation of diffusion-weighted MR imaging with cellularity of renal tumours. *Anticancer Res* 2004;24:4175-4179
13. de Bondt RB, Hoeberigs MC, Nelemans PJ, Deserno WM, Peutz-Kootstra C, Kremer B, et al. Diagnostic accuracy and additional value of diffusion-weighted imaging for discrimination of malignant cervical lymph nodes in head and neck squamous cell carcinoma. *Neuroradiology* 2009;51:183-192
14. Ono K, Ochiai R, Yoshida T, Kitagawa M, Omagari J, Kobayashi H, et al. Comparison of diffusion-weighted MRI and 2-[fluorine-18]-fluoro-2-deoxy-D-glucose positron emission tomography (FDG-PET) for detecting primary colorectal cancer and regional lymph node metastases. *J Magn Reson Imaging* 2009;29:336-340
15. Heo SH, Jeong YY, Shin SS, Kim JW, Lim HS, Lee JH, et al. Apparent diffusion coefficient value of diffusion-weighted imaging for hepatocellular carcinoma: correlation with the histologic differentiation and the expression of vascular endothelial growth factor. *Korean J Radiol* 2010;11:295-303
16. Kim JK, Kim KA, Park BW, Kim N, Cho KS. Feasibility of diffusion-weighted imaging in the differentiation of metastatic from nonmetastatic lymph nodes: early experience. *J Magn Reson Imaging* 2008;28:714-719
17. Park SO, Kim JK, Kim KA, Park BW, Kim N, Cho G, et al. Relative apparent diffusion coefficient: determination of reference site and validation of benefit for detecting metastatic lymph nodes in uterine cervical cancer. *J Magn Reson Imaging* 2009;29:383-390
18. Choi EK, Kim JK, Choi HJ, Park SH, Park BW, Kim N, et al. Node-by-node correlation between MR and PET/CT in patients with uterine cervical cancer: diffusion-weighted imaging versus size-based criteria on T2WI. *Eur Radiol* 2009;19:2024-2032
19. Lin G, Ho KC, Wang JJ, Ng KK, Wai YY, Chen YT, et al. Detection of lymph node metastasis in cervical and uterine cancers by diffusion-weighted magnetic resonance imaging at 3T. *J Magn Reson Imaging* 2008;28:128-135
20. Nakai G, Matsuki M, Inada Y, Tatsugami F, Tanikake M, Narabayashi I, et al. Detection and evaluation of pelvic lymph nodes in patients with gynecologic malignancies using body diffusion-weighted magnetic resonance imaging. *J Comput Assist Tomogr* 2008;32:764-768
21. Nakai G, Matsuki M, Harada T, Tanigawa N, Yamada T, Barentsz J, et al. Evaluation of axillary lymph nodes by diffusion-weighted MRI using ultrasmall superparamagnetic iron oxide in patients with breast cancer: Initial clinical experience. *J Magn Reson Imaging* 2011 [Epub ahead of print]
22. Chen JH, Ling R, Yao Q, Li Y, Chen T, Wang Z, et al. Effect of small-sized liposomal Adriamycin administered by various routes on a metastatic breast cancer model. *Endocr Relat Cancer* 2005;12:93-100
23. van den Brekel MW, Castelijns JA, Snow GB. The size of lymph nodes in the neck on sonograms as a radiologic criterion for metastasis: how reliable is it? *AJNR Am J Neuroradiol* 1998;19:695-700
24. Kim SH, Kim SC, Choi BI, Han MC. Uterine cervical carcinoma: evaluation of pelvic lymph node metastasis with MR imaging. *Radiology* 1994;190:807-811
25. Williams AD, Cousins C, Soutter WP, Mubashar M, Peters AM, Dina R, et al. Detection of pelvic lymph node metastases in gynecologic malignancy: a comparison of CT, MR imaging,

and positron emission tomography. *AJR Am J Roentgenol* 2001;177:343-348
26. Obwegeser R, Lorenz K, Hohlagschwandtner M, Czerwenka K, Schneider B, Kubista E. Axillary lymph nodes in breast cancer: is size related to metastatic involvement? *World J Surg* 2000;24:546-550
27. Som PM. Detection of metastasis in cervical lymph nodes: CT and MR criteria and differential diagnosis. *AJR Am J Roentgenol* 1992;158:961-969
28. Vandecaveye V, De Keyzer F, Vander Poorten V, Dirix P, Verbeken E, Nuyts S, et al. Head and neck squamous cell carcinoma: value of diffusion-weighted MR imaging for nodal staging. *Radiology* 2009;251:134-146
29. Kim JK, Jang YJ, Cho G. Multidisciplinary functional MR imaging for prostate cancer. *Korean J Radiol* 2009;10:535-551
30. Koh DM, Collins DJ. Diffusion-weighted MRI in the body: applications and challenges in oncology. *AJR Am J Roentgenol* 2007;188:1622-1635
31. Rahbar H, Partridge SC, Eby PR, Demartini WB, Gutierrez RL, Peacock S, et al. Characterization of ductal carcinoma in situ on diffusion weighted breast MRI. *Eur Radiol* 2011;21:2011-2019
32. Imamura T, Isomoto I, Sueyoshi E, Yano H, Uga T, Abe K, et al. Diagnostic performance of ADC for Non-mass-like breast lesions on MR imaging. *Magn Reson Med Sci* 2010;9:217-225
33. Jeh SK, Kim SH, Kim HS, Kang BJ, Jeong SH, Yim HW, et al. Correlation of the apparent diffusion coefficient value and dynamic magnetic resonance imaging findings with prognostic factors in invasive ductal carcinoma. *J Magn Reson Imaging* 2011;33:102-109
34. Kul S, Cansu A, Alhan E, Dinc H, Gunes G, Reis A. Contribution of diffusion-weighted imaging to dynamic contrast-enhanced MRI in the characterization of breast tumors. *AJR Am J Roentgenol* 2011;196:210-217
35. DeLano MC, Cooper TG, Siebert JE, Potchen MJ, Kuppusamy K. High-b-value diffusion-weighted MR imaging of adult brain: image contrast and apparent diffusion coefficient map features. *AJNR Am J Neuroradiol* 2000;21:1830-1836
36. Mulkern RV, Barnes AS, Haker SJ, Hung YP, Rybicki FJ, Maier SE, et al. Biexponential characterization of prostate tissue water diffusion decay curves over an extended b-factor range. *Magn Reson Imaging* 2006;24:563-568